# New features of swirling jets

Vladimir Shtern[a] and Fazle Hussain
*University of Houston, Houston, Texas 77204-4792*

Miguel Herrada
*University of Seville, 41012 Seville, Spain*

(Received 18 August 1999; accepted 26 July 2000)

Important new features are found for a family of swirling jets with velocity $\mathbf{v}\sim z^{-n}$, where $z$ is the distance from the jet origin. First, there is a sharp minimum of the pressure coefficient at a certain value of the swirl number $Sw$ which is nearly $n$ independent; this feature can be utilized in technological devices. Second, as $Sw$ increases, a separation zone develops, where the fluid is not at rest in the inviscid limit (contrary to the claims of recent vortex breakdown theories). These results are obtained under the boundary layer approximation for incompressible jets characterized by $n$ and $Sw=v_{\phi m}/v_{zm}$, where $v_{\phi m}$ and $v_{zm}$ are the maximal values of the swirl and longitudinal velocities at $z=\text{const}$. Unlike prior results viewed in terms of parameter $L$ (which is the $v_\phi/v_z$ ratio at the outer edge of the jet), the solution dependence on $Sw$ is found similar for both $n<1$ and $n>1$. For any $n$, (a) the pressure coefficient is minimum at $Sw\approx 0.65$; (b) two solutions exist for $Sw<Sw_f$ (fold value), none for $Sw>Sw_f$; (c) as $Sw$ decreases, the jets either consolidate near the axis or separate from it, depending on the solution branch; and (d) the flow in the separation zone tends to become swirl-free and potential. © *2000 American Institute of Physics.*
[S1070-6631(00)01311-8]

## I. INTRODUCTION

Typical features of swirling flows include the development of recirculatory zones,[1,2] two or more states occurring at the same values of control parameters,[3,4] and jump transitions between flow states.[5] Although these effects are of both fundamental and practical interest—being observed in tornadoes,[3] over delta wings of aircraft,[5] and in vortex devices[4]—there is still no consensus on the explanation of their mechanisms.

Consider, for example, a flow over a delta wing (inset in Fig. 1). Flow separation from the leading edge provides a source of vorticity (vortex sheet), which accumulates in a *core* (strips $c$ in the inset, and the bold line and the shaded area in the main plot of Fig. 1). The core develops due to the roll-up of the vortex sheet, which generates a swirl.[6] The swirl induces a pressure drop toward the axis of rotation, thus attracting other streamlines to the axis. This further focuses the swirl and the longitudinal momentum in the core, thus generating a strong swirling jet.

Figure 1 also schematically shows the dependence of the longitudinal velocity ($U_c$ scaled by the free stream velocity $U_\infty$) and pressure ($p_c$ scaled by the atmospheric pressure $p_\infty$) on the distance from the wing tip ($s$ scaled by its length over the wing) along the core. The velocity increases and the pressure drops in region I (jet formation). First, these effects saturate, due to (turbulent) diffusion of vorticity from the core, and then $U_c$ decreases and $p_c$ rises in region II (formation of annular jet; see below). The flow reverses (i.e., $U_c<0$) in region III (vortex breakdown ''bubble''), and, finally, $U_c$ and $p_c$ recover to $U_\infty$ and $p_\infty$ in region IV (vortex wake).

Since the vortex lift occurs because pressure above the wing is smaller (due to the vortex) than pressure below the wing, an increase in the area of low pressure can significantly enhance the lift. One goal of this paper is to examine what flow pattern corresponds to the pressure minimum. This knowledge, along with proper control methods (e.g., using winglets and blowing), can help to expand the region of low pressure and thus to increase the vortex lift of delta wings and to intensify adiabatic cooling caused by pressure drop in vortex refrigerators.

Another goal of this paper concerns a fundamental problem of vortex breakdown. The main difficulty of inviscid theories is that neither the Bernoulli head nor the circulation in a vortex breakdown ''bubble'' can be predicted. Previous attempts to overcome this indeterminacy have involved conjectures (i) that a fluid in the bubble is stagnant or (ii) that the head and circulation inside the bubble are analytical continuations of those outside. Here we examine whether these conjectures are valid for swirling jets by studying the features of viscous solutions, as viscosity tends to zero.

Both for applications and for fundamental aspects of the problem, similarity solutions are helpful, because they reduce the problem to ordinary differential equations, allowing drastically simpler and parametric analyses. This simplicity comes at a price: the solutions can model only certain regions of practical flows, e.g., away from boundaries and stagnation points. Despite this limitation, similarity solutions allow wide parametric analyses and, thus, describe many flows, show common features, and illuminate their physical reasons. For example, conical solutions (where the velocity

[a]Electronic mail: mece21w@jetson.uh.edu

 

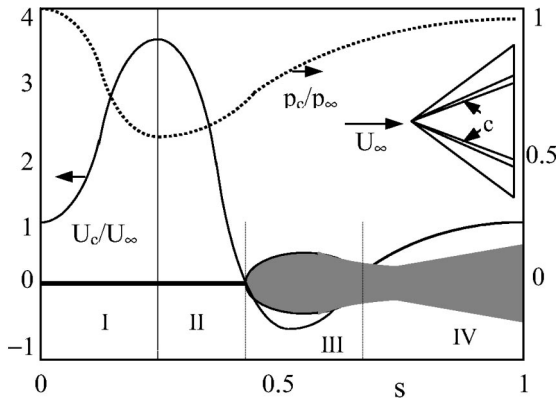


FIG. 1. Schematic of distribution of the longitudinal velocity (curve $U_c/U_\infty$) and pressure (curve $p_c/p_\infty$) along the vortex core ($c$ in inset, and the bold line and the shaded region in the main plot) over a delta wing. The core develops into a swirling jet in region I, the jet is annular in region II, region III is a vortex breakdown bubble, and region IV is a vortex wake.

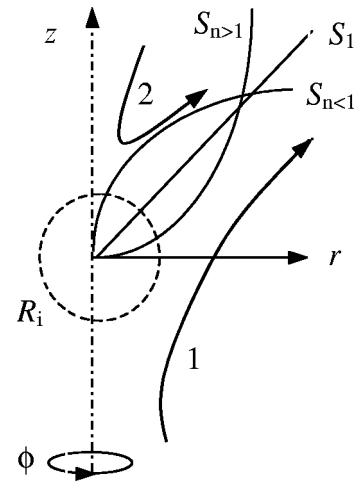


FIG. 2. Schematic of the problem: the meridional sections of typical stream surfaces (curves 1 and 2) and separating surface $S$ (the subscripts indicate values of $n$).

is inversely proportional to the distance from the origin) reveal the development of flow reversal, the nonuniqueness of flow states, and hysteretic transitions.[3,7,8]

Long[7] was the first to study conical swirling jets in the boundary layer approximation and to find a fold catastrophe: two solutions exist for $M>M_f=3.74$, one solution exists for $M=M_f$, and no solution exists for $M<M_f$; $M$ is the flow force divided by the square of the circulation and $M_f$ is the value of $M$ at the fold. Burggraf and Foster[3] interpreted this feature in terms of vortex breakdown and related it to abrupt transitions between flow states observed in tornadoes.

The mechanism of abrupt transitions was explained using conical solutions of the full Navier–Stokes equations.[8] In particular, flow reversal was found to occur even in a creeping flow, while hysteresis appears through a cusp catastrophe as Reynolds number Re exceeds some threshold value. This value is sufficiently large for the asymptotic approach (i.e., $\mathrm{Re}\to\infty$) to be applicable. This limiting case allows analytical solutions which reveal reasons for fold bifurcation and hysteresis.

An advantage of the asymptotic approach is that the Euler and boundary layer equations admit a more general family of similarity solutions than do the Navier–Stokes equations. The study of swirling flows in the boundary layer approximation has a long history.[9] Hall[10] treated vortex breakdown as a failure of the quasicylindrical (i.e., boundary layer) approach for near-axis flows—the effect being similar to that in flow separation from a wall. However, away from stagnation points, *self-similar* boundary layer solutions can describe flow reversal as found by Long[7] for the $\mathbf{v}\sim 1/z$ flows; $z$ is the distance from the jet origin.

Fernandez-Feria *et al.*[11] extended the Long jet[7] to the $\mathbf{v}\sim 1/z^n$ flows. This significant advance (like the Falkner–Skan generalization of the Blasius flow) allows the modeling of a larger number of practical flows in comparison with the Long solution. Figure 2 shows a schematic of the meridional motion for a two-cell swirling flow described by the $\mathbf{v}\sim 1/z^n$ solutions. The cylindrical coordinates $(r,\phi,z)$ are used here with $r$ scaled to blow up the vicinity of the axis of symmetry, $z$. Curves 1 and 2 are typical streamlines in the flow cells separated by a surface of revolution, which is conical at $n=1$ (line $S_1$). Curves $S_{n>1}$ and $S_{n<1}$ show the meridional section ($\phi$=const) of this separating surface (boundary of the recirculatory zone) for the $n>1$ and $n<1$ cases, respectively.

Since the $\mathbf{v}\sim 1/z^n$ solutions are singular at $z=0$ for $n>0$, they cannot model a realistic flow in the vicinity of a stagnation point, say, inside a sphere of radius $R_i$ in Fig. 2. Nevertheless, the solutions provide satisfactory local approximations of realistic flows both upstream and downstream of the stagnation point. For example, upstream of the vortex breakdown position above a delta wing, the vortex-core flow is a strong swirling jet, with its maximum longitudinal velocity five times the free stream velocity.[12] The $\mathbf{v}\sim 1/z^n$ one-cell solutions with $n>1$ can approximate the vicinity of vortex core where the flow accelerates from the free-stream to maximum velocity (see Sec. VIII). Downstream of vortex breakdown, two-cell solutions with $n\geqslant 1$ locally approximate bubblelike and conical recirculatory zones. Two-cell solutions with $n<1$ help model the outflow of vortex suction devices where a concave surface separates flow cells.[8]

Comparison of these solutions with experiment (and with other models) and better understanding of swirling flows require that relevant control parameters be used (as is known, proper scaling can cause data to collapse). Here we argue that the swirl number $Sw$ is the proper parameter for swirling jets and, especially, for the $\mathbf{v}\sim 1/z^n$ solutions. Long's parameter $M$ is suitable for the $n=1$ jets only. Fernandez-Feria *et al.*[11] use a different parameter, $L$, which is the swirl/longitudinal velocity ratio at the outer edge of the boundary layer. The choice of $L$ is inappropriate.

First, $L$ is not applicable for $n=1$ because $L(=\sqrt{2})$ is independent of $M$, and therefore $L$ fails to specify the flow in this case. Second, it is difficult to precisely locate the outer edge of a boundary layer in practical flows. Third, in terms of $L$, the results look odd: two solutions exist for $L>L_f$ and no solution exists for $L<L_f$ when $1<n<2$, while two solu-

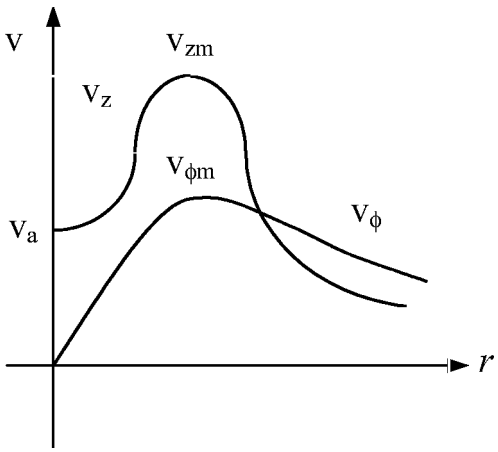


FIG. 3. Typical profiles of the axial $v_z$ and swirl $v_\phi$ velocities at a fixed $z$.

tions exist for $L<L_f$ and no solution exists for $L>L_f$ when $0<n<1$ (folds, which Fernandez-Feria *et al.*[11] interpreted as vortex breakdown).

We propose another characteristic—*swirl number* $Sw=v_{\phi m}/v_{zm}$, where $v_{zm}$ and $v_{\phi m}$ are maximal values of the longitudinal and swirl velocities at a fixed $z$ (Fig. 3). Similar to $M$ and $L$, $Sw$ is a flow parameter independent of $z$ and of viscosity $\nu$. However in contrast to $M$ and $L$, $Sw$ is relevant for the entire $\mathbf{v}\sim 1/z^n$ family. Other significant advantages are that (i) $Sw$ can be easily extracted from experimental data, unlike $M$ and $L$, and (ii) $Sw$ is a convenient parameter for local comparison of the $\mathbf{v}\sim 1/z^n$ solutions with nonsimilar flows (where $Sw$ depends on $z$).

The goal of this paper is to show that the $\mathbf{v}\sim 1/z^n$ flows have features *common* for any $n$ in terms of $Sw$. These features are (a) sharp minimum of the pressure coefficient at nearly the same value of $Sw$, (b) similar twofold dependence of the solutions on $Sw$, (c) different flow patterns on the fold branches, and (d) the development of a potential swirl-free flow in the separation zone. Note that feature (d) contradicts the analytical continuation and stagnation-zone conjectures used in inviscid theories of vortex breakdown (as discussed in Sec. VII).

To this end, we formulate the problem in Sec. II, introduce suitable parameters (Sec. III), describe new features of Long's jet (Sec. IV), show that these features are common for the $n>1$ and $n<1$ jets as well (Sec. V), describe how a potential flow develops in the separation zone (Sec. VI), compare the features of similarity jets with inviscid theories of vortex breakdown (Sec. VII) and with experiment (Sec. VIII), and summarize our new results (Sec. IX).

## II. PROBLEM FORMULATION

To simplify the analysis, we modify the problem formulation by Fernandez-Feria *et al.*[11]

### A. Governing equations

The boundary layer equations for a near-axis rotationally symmetric flow of a viscous incompressible fluid in the cylindrical coordinates $(r,\phi,z)$,[9]

$$\begin{aligned}
&\partial(rv_r)/\partial r+\partial(rv_z)/\partial z=0, \quad \rho\Gamma^2/r^3=\partial p/\partial r,\\
&v_r\partial\Gamma/\partial r+v_z\partial\Gamma/\partial z=\nu r\partial/\partial r(r^{-1}\partial\Gamma/\partial r),\\
&v_r\partial v_z/\partial r+v_z\partial v_z/\partial z=-\rho^{-1}\partial p/\partial z+\nu r^{-1}\partial(r\partial v_z/\partial r)/\partial r,
\end{aligned} \tag{1}$$

admit the similarity solutions,

$$\begin{aligned}
&v_z=2\nu z\delta^{-2}f'(\xi), \quad \Gamma=2^{1/2}\nu z\delta^{-1}\gamma(\xi),\\
&v_r=\nu r^{-1}(2\xi f'/m-f), \quad m=2-n,\\
&p=p_\infty+\rho(\nu z)^2\delta^{-4}\beta(\xi), \quad \xi=(r/\delta)^2,\\
&\delta=2^{1/2}zm^{1/m}(\Gamma_\infty z^{m-1}/\nu)^{-1/m}.
\end{aligned} \tag{2}$$

Here $\Gamma=rv_\phi$, $\rho$ is the density, $\nu$ is the kinematic viscosity, $(v_r,v_\phi,v_z)$ are the velocity components, $\delta\sim z^{1/m}$ is the boundary layer thickness, the prime denotes differentiation with respect to $\xi$, $\Gamma_\infty z^{m-1}/\nu$ is a kind of Reynolds number, and $\Gamma_\infty$ is a dimensional constant. In the particular case $n=m=1$, $\Gamma_\infty$ is a circulation value far away from the axis: $\Gamma\to\Gamma_\infty$ as $\xi\to\infty$. The dimensionless functions $\beta$, $\gamma$, and $f$ replace pressure $p$, circulation $\Gamma$, and the Stokes stream function $\Psi=\nu zf$, respectively.

Substituting (2) in (1) yields the ordinary differential equations

$$\begin{aligned}
&\xi^2\beta'=\gamma^2,\\
&2\xi\gamma''=(1-1/m)\gamma f'-f\gamma',\\
&2(\xi f'')'+(2/m-1)f'^2+ff''+(2m)^{-1}\\
&\quad\times[(2-m)\beta+\gamma^2/\xi]=0.
\end{aligned} \tag{3}$$

Note that $\gamma$ here, in contrast to $\gamma_F=(2/\xi)^{1/2}\gamma(\xi)$ used by Fernandez-Feria *et al.*,[11] is an analytical function of $\xi$; this feature of $\gamma$ eases calculations because both the equations (3) and the boundary conditions (described below) are simpler than those in Ref. 11.

### B. Boundary conditions

The requirement that the viscous terms in (3) become negligible as $\xi\to\infty$ yields

$$f\to\xi^{m/2} \quad \text{and} \quad 2\xi\gamma'+(m-1)\gamma\to 0 \quad \text{as} \quad \xi\to\infty. \tag{4}$$

The requirement that the velocity is bounded on the axis, $\xi=0$, yields

$$\begin{aligned}
&f=0, \quad \gamma=0, \quad \text{and}\\
&2f''+(2/m-1)f'^2+(2m)^{-1}(2-m)\beta=0 \quad \text{at} \quad \xi=0.
\end{aligned} \tag{5}$$

In addition, we use the condition

$$f'(0)=f_1, \tag{6}$$

where $f_1$ is an intermediate free parameter. Equations (3) and boundary conditions (4)–(6) constitute a closed mathematical problem.

### C. Numerical procedure

Depending on parameter values, we use two algorithms to solve the problem numerically. In the first algorithm, integration starts from $\xi=0$ with conditions (5) and (6) and

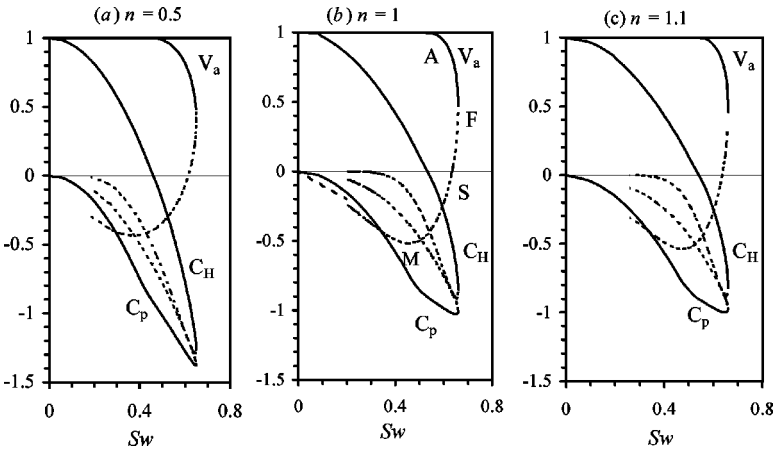


FIG. 4. Dependence of $V_a = v_a/v_{zm}$ and pressure ($C_p$) and head ($C_H$) coefficients on swirl number $Sw$ for (a) $n=0.5$, (b) $n=1$, and (c) $n=1.1$.

guessed values of $\beta(0)$ and $\gamma'(0)$. Resolving the 0/0 indeterminacies in (3) yields the highest derivatives at $\xi=0$, as follows:

$$f''' = [(1-4/m)f'f'' - (2m)^{-1}[(2-m)\beta' + \gamma'^2]]/4,$$

$$\beta' = \gamma'^2 \quad \text{and} \quad \gamma'' = -1/(2m)\gamma' f'.$$

The integration runs from $\xi=0$ to $\xi=\xi_f$ (typically we take $\xi_f = 10^4$), and then $\gamma'(0)$ and $\beta(0)$ are adjusted (with the help of the Newton shooting procedure) to satisfy (4) at $\xi=\xi_f$.

The second algorithm is for two-cell flows where the inter-cell boundary, $\xi=\xi_s$, is far from the axis ($\xi_s \gg 1$). In this case, we integrate (3) from $\xi=\xi_s$ in both directions, to $\xi=0$ and to $\xi=\xi_f$, using $f(\xi_s)=0$, $f'(\xi_s)=f_1$, and guessed values of $f''$, $\beta$, $\gamma$, and $\gamma'$ at $\xi=\xi_s$. Then the guessed values are adjusted to satisfy (4) (at $\xi=\xi_f$) and (5).

After solving the problem, we calculate the parameters described below, which characterize important kinematic and dynamic features of swirling jets.

## III. COMMON PARAMETERS OF SWIRLING JETS

To compare the $n>1$, $n=1$, and $n<1$ solutions (whose features were found by Fernandez-Feria *et al.*[11] to differ markedly in terms of $L$), we introduce new flow characteristics. Fortunately, swirling jets allow suitable common parameters based on their similar features in velocity and pressure distributions. An important characteristic is the swirl number $Sw = v_{\phi m}/v_{zm}$ (introduced in Sec. I) which we use as a *control* parameter. Recall that $v_{\phi m}$ is the maximum swirl velocity at $z=\text{const}$ (Fig. 3); the maximum location indicates a boundary of the vortex core of the swirling motion in the consolidated jets. The $Sw$ value shows the strength of the swirl compared with the meridional motion within the jet. Since the maximum longitudinal velocity at $z=\text{const}$ is not necessarily located at $r=0$, one useful *resultant* characteristic is $V_a = v_a/v_{zm}$, where $v_a$ is the velocity on the axis (Fig. 3).

Both $V_a$ and $Sw$ describe only the flow kinematics; we also apply the pressure coefficient $C_p$ to characterize the flow dynamics. A strong drop in pressure is typical of swirling jets and contributes to the vortex lift of delta wings and to the refrigerating (Ranque) effect in vortex tubes. Here this important feature is accounted for by $C_p = (p_a - p_\infty)/e_m$; $p_a$ and $p_\infty$ are pressure values both on, and far away from, the axis, while $e_m$ is the maximum of the local kinetic energy, $e = \rho v^2/2$, at a fixed $z$. Therefore, $C_p$ estimates the pressure drop per unit dynamic head. In addition, we use $C_H = (p_a - p_\infty + \rho v_a^2/2)/e_m$ to evaluate the hydraulic head on the axis. Although $p_a - p_\infty$, $e_m$, and $v_a$ are functions of $z$, $C_p$ and $C_H$ are $z$ independent and therefore $C_p$ and $C_H$ are global characteristics of the $\mathbf{v} \sim 1/z^n$ flows. These parameters can be calculated for nonsimilar flows (e.g., for swirling flows above delta wings, in tubes, and in vortex chambers) as well and, in addition, these parameters can be easily measured experimentally. In nonsimilar flows, however, $V_a$, $Sw$, $C_p$, and $C_H$ vary with $z$, in contrast to the similarity jets studied here.

## IV. NEW FEATURES OF THE LONG JET

It is instructive first to reconsider the $n=1$ solutions in terms of the new parameters. Figure 4 shows that the dependence of $V_a$, $C_p$, and $C_H$ on $Sw$ is twofold. The curve $V_a(Sw)$ has three characteristic points. Along the upper branches, $V_a=1$ for small $Sw$. This corresponds to a consolidated jet with the maximum, $v_{zm}$, located on the axis of symmetry (e.g., see Fig. 13). Such a velocity distribution is typical of swirling flows well upstream of vortex breakdown.[12]

As $Sw$ increases beyond some threshold value, the maximum of $v_z$ moves away from the axis; there is now a local *minimum* of $v_z$ (Fig. 5). Thus, $V_a$ becomes less than 1, e.g., while passing point $A$ as $Sw$ increases along the upper branch of curve $V_a(Sw)$ in Fig. 4(b); symbol $A$ denotes the transformation of a consolidated jet (where $V_a=1$) into an *annular* jet (where $V_a<1$). Annular jets occur upstream,[13] downstream,[14] and between[15] vortex breakdown bubbles.

Moving further along curve $V_a(Sw)$ in Fig. 4, we encounter a qualitative change in flow pattern when $V_a$ becomes negative (e.g., see the $v_z$ profile in Fig. 8). The flow reverses near the axis and becomes two-cellular (Fig. 2). The flow reversal occurs at point $S$ in Fig. 4(b); symbol $S$ denotes flow *separation* from the axis.

On the curves in Fig. 4(b), $Sw$ reaches its maximum $Sw_f = 0.661$ at the *folds*, e.g., at point $F$ where $V_a = 0.447$ on curve $V_a(Sw)$. If $Sw$ increases beyond its fold value $Sw_f$,

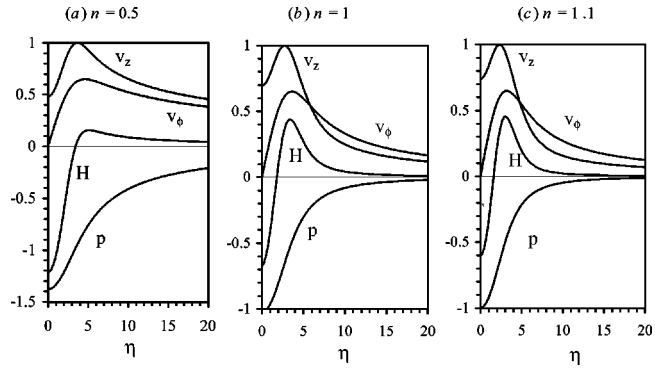


FIG. 5. Profiles of velocities $v_z$ and $v_\phi$, pressure $p$, and head $H$, corresponding to the $C_p$ minimum in Fig. 4.

the flow abruptly transforms into a very different state (which differs from the near-axis jet and therefore requires another approach, see Refs. 8 and 16).

On the lower branch of curve $V_a(Sw)$, $V_a$ reaches its minimum at point $M$ in Fig. 4(b), where the reversed flow is the strongest. As $Sw \to 0$ along the lower branch, $V_a$ also tends to zero approaching the asymptote $V_a = -Sw$ shown by the broken line in Fig. 4(b); this asymptote follows from the analytical solution found in Ref. 8.

Note that as $Sw \to 0$ along the lower branch of curve $V_a(Sw)$ in Fig. 4(b), the location of the $v_z$ maximum moves far away from the axis (see Sec. VI), rendering the boundary layer approach invalid. The boundary layer approach also fails to capture other folds and solution branches described by the full Navier–Stokes equations.[8]

Despite these limitations, the boundary layer approach helps us to reveal a new important feature of near-axis jets—the existence of the $C_p$ minimum, as Fig. 4 shows. In Fig. 4(b), the minimum of $C_p(=-1.027)$ occurs in the annular jet without flow reversal [Fig. 5(b)] at $Sw = 0.6515$ and $V_a = 0.696$, a point located on curve $V_a(Sw)$ above the fold. The finding of the velocity profiles and $Sw$ at which $C_p$ reaches its minimum can be utilized to enhance the vortex lift of delta wings and to achieve the deepest adiabatic cooling in the Ranque tubes. To this end, the flow region containing the $C_p$ minimum should be appropriately enlarged in each device—for example, by proper blowing on delta wings, and by shaping the side wall of vortex tubes.

The $C_p$ minimum has a clear physical reason. As $Sw \to 0$ along the lower branch of curve $C_p$ (note that the upper branch of curve $V_a$ corresponds to the upper branch of curve $C_H$, but to the lower branch of curve $C_p$ in Fig. 4), the jet tends to the Schlichting (swirl-free) jet (this limiting transition is uniform for velocity, but is not uniform for stream function). Pressure is constant across this jet; more precisely, $p_a - p_\infty$ is a small positive quantity proportional to $\mathrm{Re}^{-1}$. This yields that $C_p \to 0$ and $C_H \to 1$ as $Sw \to 0$ (see the lower branch of curve $C_p$ and the upper branch of curve $C_H$ in Fig. 4). In contrast, $p_a - p_\infty$ is negative in jets with strong swirl, a consequence of cyclostrophic balance.

As $Sw$ decreases along the other branch, the maximum of $v_\phi$ moves away from the axis and its value decreases [e.g., see Figs. 8(a) and 8(b)]. Since $p_\infty - p_a = \int_0^\infty (\rho v_\phi^2/r)dr$, this yields a decrease in $p_\infty - p_a$, and thus again $C_p \to 0$ as $Sw \to 0$. Therefore, $C_p$ reaches its (negative) minimum at a certain $Sw$ (which appears to be very close to $Sw_f$).

It is interesting that $C_H$ also tends to zero along the lower branch of curve $V_a$, even more rapidly than does $C_p$. A reason is that the flow becomes irrotational inside the near axis cell (see Sec. VI) where the head is constant and equal to its ambient value, i.e., $C_H = 0$. We show in Sec. V that a similar effect occurs in the $n \neq 1$ flows as well.

It is important to know what flow pattern corresponds to the $C_p$ minimum. Figure 5 shows the velocity components, $v_z$ and $v_\phi$, pressure $p$, and head $H = p - p_\infty + \rho v^2/2$ as functions of $\eta = \xi^{1/2} = r/\delta$ (which is a scaled polar angle) at a fixed $z$. Here $v_z$ and $v_\phi$ are normalized by $v_{zm}$, while $p$ and $H$ are normalized by $e_m$, all of which served to make the curves in Fig. 5 $z$ independent. It is interesting that at the $C_p$ minimum, $v_z$, $v_\phi$, and $H$ have their maxima at nearly the same distance from the axis.

Near the axis, the pressure drop exceeds the kinetic energy providing the negative total head $H$ for small $\eta$. As one moves away from the axis, the pressure drop decreases while the kinetic energy increases, causing the $H$ growth and change in sign. As $\eta$ further increases, passing the $e_m$ location (near the $v_z$ maximum in Fig. 5), $H$ decreases. Far away from the axis, $H$ becomes negligibly small compared with its characteristic values inside the vortex core.

## V. COMPARISON WITH THE $n \neq 1$ FLOWS

Figures 4 and 5 show that the results for $n = 0.5$ (a), $n = 1$ (b), and $n = 1.1$ (c) are qualitatively the same. Even numerical values of key characteristics are similar. For example, the minimum of $C_p = -0.998$ occurs at $Sw = 0.6495$ and $V_a = 0.740$ for $n = 1.1$; these numbers are very close to those for $n = 1$. For $n = 0.5$, the minimum of $C_p = -1.378$ occurs at $Sw = 0.649$ and $V_a = 0.483$. Interestingly, the $Sw$ value corresponding to the $C_p$ minimum is nearly invariant, although $C_p$ and $V_a$ vary remarkably.

It is instructive to compare $C_p$ for the $\mathbf{v} \sim z^{-n}$ jets with $C_p$ for the Rankine vortex, a widely used reference case.[17–19] The Rankine vortex is an exact solution of the Euler equations where the swirl velocity depends only on $r$, viz.:

$$v_\phi = v_{\phi m} r/r_c \quad \text{for } r \leq r_c \quad \text{and } v_\phi = v_{\phi m} r_c/r \quad \text{for } r_c \leq r < \infty.$$

The pressure distribution in the Rankine vortex is

$$p = p_\infty - \rho v_{\phi m}^2 (1 - \tfrac{1}{2} r^2/r_c^2) \quad \text{for } r \leq r_c$$

and

$$p = p_\infty - \tfrac{1}{2} \rho v_{\phi m}^2 r_c^2/r^2 \quad \text{for } r_c \leq r < \infty.$$

This yields $C_p = -2$ ($Sw$ and $V_a$ are not applicable since $v_z = 0$ in the Rankine vortex).

As the Rankine vortex is $z$ independent, it corresponds to $n = 0$ in the $\mathbf{v} \sim z^{-n}$ family of similarity solutions. Our results show that the $C_p$ minimum decreases with $n$, and, as $n \to 0$, $C_p$ tends to $-2$, i.e., to its value for the Rankine vortex. (However, note that if we scale the pressure drop, $p_a - p_\infty$, using not the total kinetic energy $e_m$ but the swirl kinetic

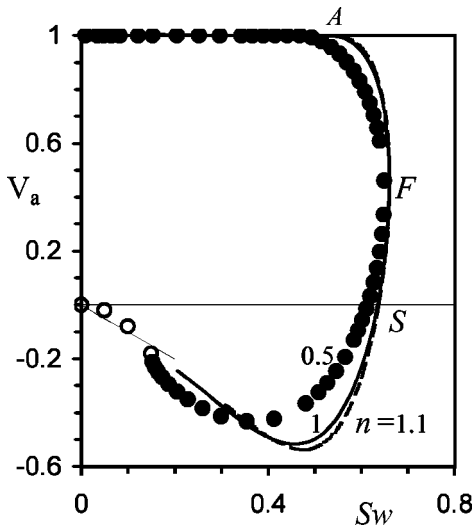


FIG. 6. Comparison of curves $V_a(Sw)$ for the $n$ values shown near the curves.

energy $\frac{1}{2}\rho v_{\phi m}^2$, then this modified pressure coefficient would be nearly $Sw^{-2}$ times $C_p$.) In practical vortex chambers near the endwall where a swirling jet develops, a typical value of the $C_p$ minimum, $C_{pm}$, is close to $-1$ (which corresponds to $n \approx 1$ in the the $\mathbf{v} \sim z^{-n}$ family), although $C_{pm}$ depends on the chamber geometry.[20,21]

To clearly demonstrate that the swirling jets have common features for $n>1$, $n=1$, and $n<1$, Fig. 6 gathers the $V_a(Sw)$ data for $n=0.5$, 1, and 1.1. The curves are obviously quite similar. The most significant difference occurs in the vicinity of $Sw=V_a=0$. The $n=1$ curve has the linear asymptote, $V_a=-Sw$, while the derivative of function $V_a(Sw)$ at $Sw=0$ seems to be zero for $n<1$ and infinite for $n>1$. However, the boundary layer approach is invalid in the vicinity of $Sw=V_a=0$ (as discussed in Sec. IV).

Figure 7 shows the cumulative results on the parameter plane $(n,Sw)$. Curves $F$, $S$, and $A$ are projections of the

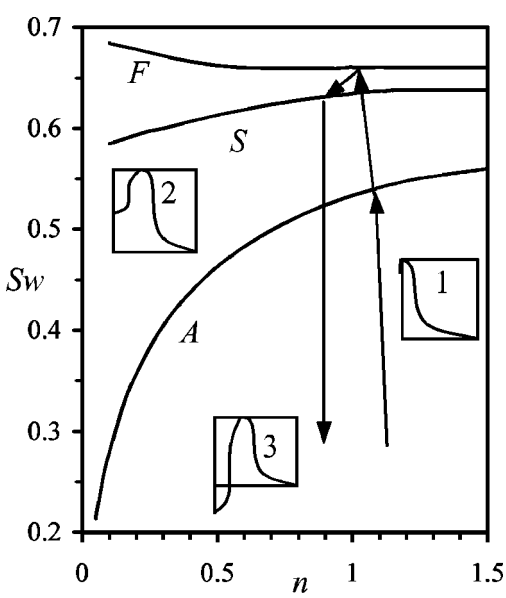


FIG. 7. Map of flow states on the parameter plane.

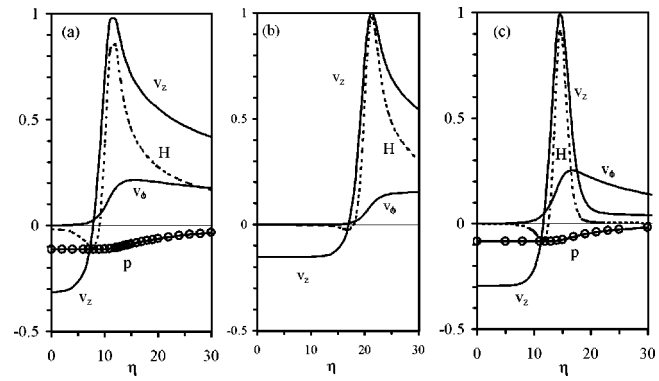


FIG. 8. Profiles for the two-cell flow at (a) $n=0.5$ and $Sw=0.203$, (b) $n=0.5$ and $Sw=0.117$, and (c) $n=1.1$ and $Sw=0.246$.

corresponding points [e.g., as shown in Figs. 4(b) and 6] and indicate fold ($F$), flow separation ($S$), and the transition from consolidated jets to annular jets ($A$). According to the two-branch curves in Fig. 6, the plane in Fig. 7 is twofold, as the arrows illustrate. As $Sw$ increases along the lower arrow directed upward, the jet is consolidated; inset 1 shows a profile of $v_z(r)$ at a fixed $z$. Along the next two arrows, the jet is annular with a *positive* minimum of $v_z$ at the axis (inset 2). Along the last (downward) arrow, the flow is two cellular and $v_z$ has a *negative* minimum on the axis (inset 3). If $Sw$ decreases further, the flow becomes irrotational near the axis, as discussed below in more detail.

## VI. DEVELOPMENT OF A POTENTIAL FLOW IN THE SEPARATION ZONE

While it is known that the inviscid flow is swirl-free and potential in the near-axis cell of two-cell flows (see Refs. 8 and 22 for $n=1$ and Ref. 16 for $n \neq 1$), we show below how this feature appears as $Sw$ varies. Figures 8(a) and 8(b) depict the profiles for the lower branch of the $n=0.5$ curve in Fig. 6 and for (a) $Sw=0.203$, $\eta_s=10$ and (b) $Sw=0.117$, $\eta_s=20$; $\eta=\eta_s$ is the boundary of the separation zone where the stream function is zero, $f(\eta_s)=0$. Comparison of Figs. 8(a) and 8(b) clearly demonstrates that, as $Sw$ decreases, (i) the width of the separation zone increases, (ii) $v_\phi$ and $H$ vanish near the axis, and (iii) $v_z$ becomes uniform in the reversed flow. We do not show the $p$ distribution in Fig. 8(b) because the pressure drop is so small ($C_p=-0.023$) that the corresponding curve nearly merges with the zero line. Thus, the flow becomes irrotational near the axis as the separation zone expands for the $n<1$ solutions. Figure 8(c) shows the similar profiles at $n=1.1$, $Sw=0.246$ ($\eta_s=14.3$). Again, $v_\phi$ and $H$ vanish while $v_z$ is uniform in the reversed flow.

It is striking that the reversed flow can remain irrotational even in a very narrow separation zone. We find this effect for the $n>1$ solutions. Figure 9 shows the dependence of the thickness $\eta_s$ of the separation zone on $Sw$ along the lower branch of the $V_a(Sw)$ curve for $n=1.1$ [Fig. 4(c)]. As $Sw$ decreases, $\eta_s$ first increases up to $\eta_s=14.37$ at $Sw=0.24$ and then decreases. Figure 10 shows the velocity profiles for the solutions with the same $\eta_s=5$ at (a) $Sw=0.515$ and (b) $Sw=0.158$ (see Fig. 9). In the separation

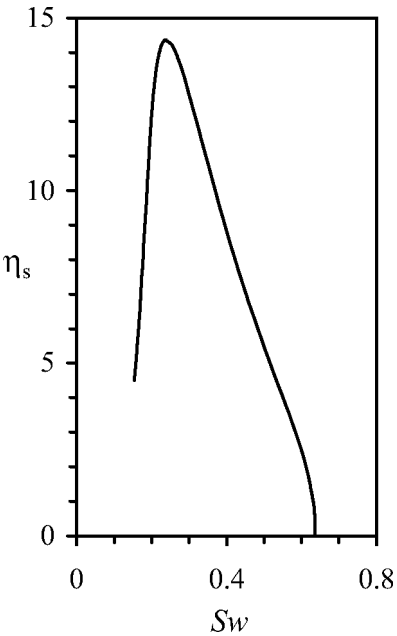


FIG. 9. Thickness $\eta_s$ of the near-axis cell versus $Sw$ along the lower branch of the $V_a(Sw)$ curve in Fig. 4(c).

zone, the flow is vortical in Fig. 10(a), but potential in Fig. 10(b) where the jet is very thin and the flow reverses on both sides of the jet. As $Sw$ further decreases, the jet becomes a viscous sublayer of a significantly smaller thickness than that of the basic boundary layer; in particular, the distance between the $v_z$ zeroes [Fig. 10(b)] becomes small compared with $\eta_s$. Presumably, this developing singularity as $Sw \to 0$ indicates that the flow becomes nonsimilar.

Thus we have found that $\eta_s$ is limited for $n>1$, but grows without a limit for $n \leqslant 1$. This agrees with the results by Fernandez-Feria *et al.*[16] that the potential flow of the $O(1)$ thickness can be matched with an outer vortical flow only for $n \leqslant 1$. In the $n>1$ case, no boundary layer solution (from the $\mathbf{v} \sim 1/z^n$ family) exists which can match these flows. Here we have revealed two reasons for this feature of

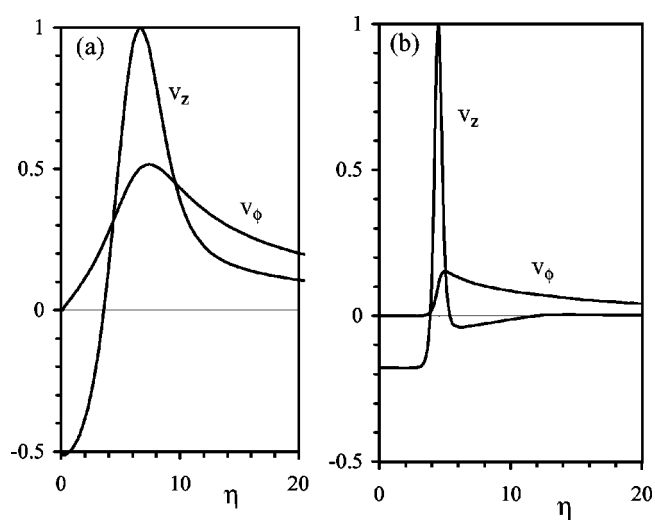


FIG. 10. Velocity profiles at $n=1.1$ and $\eta_s=5$ for (a) $Sw=0.515$ and (b) $Sw=0.153$.

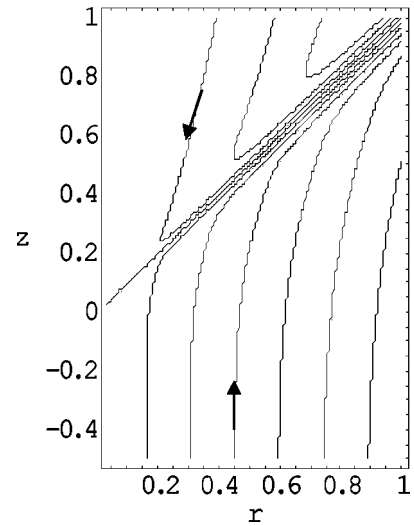


FIG. 11. Meridional section ($\phi$=const) of stream surfaces for solution (7) at $x_s=0.707$.

the $n>1$ inviscid flows: (i) the thickness of the separation zone is limited to the viscous scale (e.g., $\eta_s<15$ at $n=1.1$), and (ii) the viscous sublayer develops within the near-axis boundary layer.

It can thus be seen that the tendency for the reversed flow to become irrotational occurs for both the $n<1$ solutions and the $n>1$ solutions. For the $n=1$ flows, this effect is well known: it was found first in the Long boundary layer[22] and then for solutions of the full Navier–Stokes equations.[8] To discuss this effect, we address here the particular entire-domain flow which is relevant in the context of this paper. To imitate the delta-wing vortex, consider a flow induced by a half-line vortex of circulation $\Gamma_0$ located at the negative $z$ axis in an infinite fluid. The vortex singularity models a consolidated part of the vortex, upstream of vortex breakdown. The flow downstream can be either consolidated or two cell. As $\mathrm{Re}=\Gamma_0/\nu \to \infty$, the analytical solution for the two-cell flow is as follows:[8]

$$\gamma=1, \quad \psi=\tfrac{1}{2}\{(1+x)[3x_s+1-(3+x_s)x]/(1+x_s)\}^{1/2},$$
$$q=-\tfrac{1}{4}[3x_s+1-(1-x_s)x]/[(1+x_s)(1-x^2)]$$
$$\text{for } -1<x<x_s,$$

and

$$\gamma=0, \quad \psi=-\tfrac{1}{2}(1-x)[(1+x_s)/(1-x_s)]^{1/2},$$
$$q=-\tfrac{1}{4}(1+x_s)(1-x_s)^{-1}(1-x)^{-1} \quad \text{for } x_s<x<1. \tag{7}$$

Here, $\gamma=\Gamma/\Gamma_0$, $\psi=\Psi/(r_{sp}\Gamma_0)$, $x=z/r_{sp}$, $r_{sp}=(r^2+z^2)^{1/2}$, and $x=x_s$ is a conical surface separating the cells. Figure 11 shows streamlines of the meridional motion at the separating angle $\theta_c=45°$ ($x_s=\cos\theta_c$). The near-axis cell in Fig. 11 resembles the conical breakdown observed by Sarpkaya[23] (for $n \neq 1$, the separating surface $S$ is curved, as shown in Fig. 2). Solution (7) explicitly demonstrates that in the separation zone ($x_s<x \leqslant 1$), the swirl is absent and the meridional motion is potential. Fernandez-Feria *et al.*[16] proved that the flow must be potential in the near-axis cell of

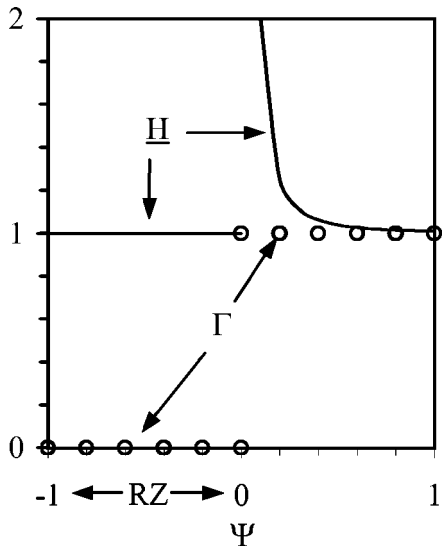


FIG. 12. Typical dependence of head $H$ and circulation $\Gamma$ on stream function $\Psi$ for the $\mathbf{v}\sim 1/z^n$ flows inside ($\Psi<0$) and outside ($\Psi>0$) recirculation zone RZ.

two-cell solutions of the Euler equations for the $n\neq 1$ flows as well. Thus, this feature is valid not only for the near-axis boundary layers (as shown in this section) but also for full-domain flows. Now we compare this fact with the conjectures used in inviscid theories of vortex breakdown.

## VII. COMPARISON WITH CONJECTURES MADE IN INVISCID THEORIES

The steady Euler equations for axisymmetric incompressible flows can be reduced to the form,

$$r\partial/\partial r(r^{-1}\partial\Psi/\partial r)+\partial^2\Psi/\partial z^2=r^2\,dH/d\Psi-\Gamma\,d\Gamma/d\Psi,$$

which is often referred as the Bragg–Hawthorne or Squire–Long equation (although it was used significantly earlier by Meissel[24]). Functions $H(\Psi)$ and $\Gamma(\Psi)$ are defined by inflow boundary conditions outside, but are undetermined inside, a separation zone. Some inviscid theories of vortex breakdown involve conjectures that (i) $H(\Psi)$ and $\Gamma(\Psi)$ can be analytically continued[17,25] or (ii) fluid stagnates[18,19,26] in the separation zone.

Both of these conjectures, (i) and (ii), appear invalid for the swirling flows considered here. In particular, the analytical solution (7) yields that $\Gamma=H=0$ inside the separation zone ($x_s<x<1$, where $\Psi<0$), while $\Gamma=\Gamma_0=\text{const}$ and $H=\frac{1}{2}\rho\Gamma_0^4\Psi^{-2}$ outside the separation zone ($x<x_s$, where $\Psi>0$) as $\text{Re}\to\infty$. Figure 12 illustrates this result, presenting $\underline{H}/p_\infty(\underline{H}=H+p_\infty)$ and $\Gamma/\Gamma_0$ versus $\Psi$ inside ($\Psi<0$) and outside ($\Psi>0$) the recirculatory zone (RZ).

The flow does not stagnate inside the separation zone, although $\Gamma=H=0$ there. The inviscid solutions are singular at the surface separating the cells, and there is a boundary-layer solution smoothing this singularity. The $\mathbf{v}\sim z^{-n}$ flow is vortical outside the separation zone, where $H=\frac{1}{2}K_1(m-2)^{-1}\Psi^{2-4/m}$ and $\Gamma=K\Psi^{1-1/m}$; $K_1$ and $K$ are constants.[16] These features agree with our results concerning both the entire-domain flows at $n=1$ and the near-axis jets of any $n$ (Sec. VI).

Thus, the inviscid limit reveals that (i) $H(\Psi)$ and $\Gamma_d(\Psi)$ have jumps at the boundary of separation zone—which contradicts the analytical-continuation conjecture; (ii) swirl is absent in the separation zone—which seems to agree with the stagnation-zone model; and (iii) the meridional motion in the separation zone is irrotational and is of the same magnitude as the outside the separation zone—which *contradicts* the stagnation-zone model.

The fact that the stagnation model is invalid for the $\mathbf{v}\sim 1/z^n$ flows does not necessarily mean that this model cannot be applied in other cases. For swirling flows in pipes, there are theoretical arguments,[19,26] as well as experimental evidence, in favor of the stagnation model. Note that the separation zones in the $\mathbf{v}\sim 1/z^n$ flows are semi-infinite domains which expand downstream and have jet-like flows at the boundaries. These solutions do not capture the vortex-breakdown ''bubbles'' and semi-infinite cylindrical domains typical of pipe flows. Therefore, although our results definitely reveal a limitation of the stagnation and analytical-continuation models (namely, their invalidity for the $\mathbf{v}\sim 1/z^n$ flows), these models could nonetheless be useful for other flows.

The inviscid models, however, fail to explain one important effect—the strong flow acceleration upstream of vortex breakdown and the formation of swirling jets within vortex cores above delta wings and in slightly diverging pipes. In contrast, the $\mathbf{v}\sim 1/z^n$ solutions capture this feature, as shown in Sec. VIII, where we compare the theoretical and experimental velocity distributions in the consolidated vortex core.

## VIII. COMPARISON WITH EXPERIMENT

Earnshaw measurements[27] of the velocity distribution above delta wings clearly demonstrate that the cores of leading-edge vortices are swirling jets. Upstream of vortex breakdown, the profile of the longitudinal velocity across the core peaks sharply, and the maximum velocity is nearly three times the free stream velocity. Menke and Gursul[12] confirm this observation and also state that the maximum can be even as high as five times the free stream velocity. Sarpkaya and Novak[28] find a similar effect for a swirling flow in a diverging pipe: the maximum of the longitudinal velocity in a vortex core is 3.5 times the velocity far from the core.

Such strong flow acceleration in vortex cores occurs due to the self-focusing mechanism: the swirl induces a pressure drop near the axis, thus attracting other streamlines and increasing $v_a$, and flow convergence further focuses the swirl. This positive feedback causes a vortex-sink-type accumulation of axial and angular momenta near the axis.[29] As the radial gradients of $v_z$ and $v_\phi$ increase, strong (turbulent) diffusion develops and finally balances the accumulation. The saturated value of $v_a$ depends on effective viscosity $\nu_t$: $v_a$ increases as $\nu_t$ decreases. Since turbulence (and $\nu_t$) typically diminishes in an accelerating flow, the cumulative effect can be very strong; this explains the high velocity peaks observed in experiments.

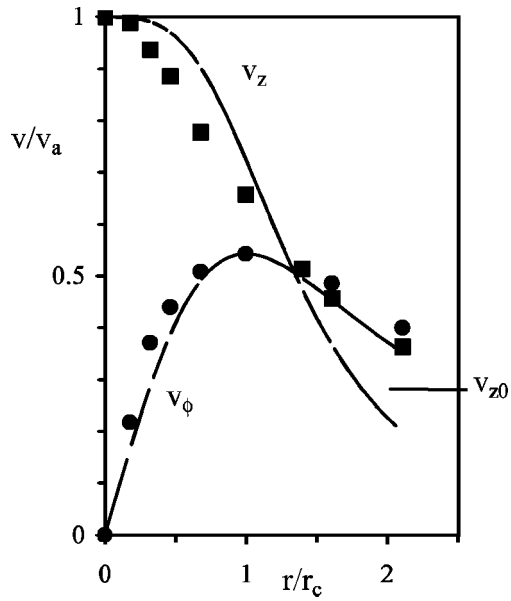


FIG. 13. Comparison of the velocity profiles from the experiment (Ref. 28) (symbols) and the theory (curves) at $n=1.233$ and $Sw=0.543$.

Taking into account the jet-like character of the core upstream of vortex breakdown, we now compare the experimental profiles of $v_z$ and $v_\phi$ with those resulting from the $\mathbf{v}\sim 1/z^n$ solutions. Comparing the laminar theory with a turbulent practical flow, we interpret $\nu$ as the uniform eddy viscosity $\nu_t$ (following Schlichting who did this for the swirl-free round jet[9]). While the theory treats rotationally symmetric flows, vortex cores above delta wings are remarkably asymmetric: the $v_\phi$ maximum on one side of the vortex axis is 1.5 times the maximum on the opposite side, according to the Menke and Gursul measurements.[12] For this reason, we here compare the theoretical profiles with the quite symmetric data by Sarpkaya and Novak: the symbols in Fig. 13 are extracted from Fig. 4(a) of their paper.[28] These $v_z$ and $v_\phi$ profiles were measured at $z/D=1.8$, i.e., substantially upstream of the vortex breakdown location at $z/D=2.8$ ($D$ being the pipe inlet diameter). The curves in Fig. 13 are the theoretical results at $n=1.233$ and $Sw=0.543$ (chosen to better fit experimental data). The velocities $v_z$ and $v_\phi$ are normalized by $v_a$, and the radial coordinate is normalized by the core radius, $r_c$, which corresponds to the $v_\phi$ maximum.

The agreement looks satisfactory inside the core, especially for swirl velocity. However, the experimental $v_z$ profile is sharper near the axis, compared with the theoretical (laminar) profile, as typical for turbulent jets.[9] One reason is that the eddy viscosity is not uniform within the core (the viscosity maximum is located away from the axis). (Our preliminary results show that the Prandtl mixing-length model, $\nu_t=l^2\, dv_z/dr$, better fits the experiment, similar to the case of the non-swirling jet.[9] However such turbulence modeling is outside the scope of this paper.) Away from the core, the experimental and theoretical results diverge. As $r/r_c$ increases, $v_z$ saturates to its ambient *nonzero* value $v_{z0}$ (see the horizontal line in Fig. 13) in the experiment, while in theory, $v_z$ goes to zero as $r/r_c\to\infty$.

Consider now the twofold character of $Sw$ for the $\mathbf{v}\sim 1/z^n$ jets in the context of experimental observations. For example, in the Sarpkaya and Novak experiment,[28] $Sw=0.54$ at $z/D=1.8$ (upstream of vortex breakdown) and $Sw=0.18$ at $z/D=4$ (downstream of vortex breakdown) in the same flow. These data give a quantitative estimate of how the flow separation affects the $Sw$ value. Above a delta wing, a local value of $Sw$ first increases (together with circulation) downstream of the wing tip, but then drops as vortex breakdown develops. Therefore, two different local flow states (upstream and downstream of vortex breakdown) have the same value of $Sw$. Thus, the twofold dependence of $Sw$ has clear physical reasons and agrees with experimental results.

The range $Sw<0.7$ (Fig. 7) is a limitation of the $\mathbf{v}\sim 1/z^n$ solutions, as $Sw$ can significantly exceed 1 in some regions of practical flows. For example, $Sw$ is of $O(10)$ for a flow induced by a rotating endwall inside a sealed cylindrical container.[30] Also, $Sw$ is large near the inlets of vortex chambers and in the Ranque tubes, where the swirl dominates the axial flow. In contrast, $Sw<1$ in the entire flow domain above delta wings, in outflows of vortex chambers and tubes, and in tornadoes, although swirl is strong in these flows. For example, vortex breakdown in the near field of swirling jets occurs at $Sw\approx 0.65-0.7$; this experimental result of Billant *et al.*[31] agrees with the fold value of $Sw$ predicted here (curve $F$ in Fig. 7).

To summarize: the $\mathbf{v}\sim 1/z^n$ solutions provide a satisfactory approximation of the velocity distribution in a vortex core, although these solutions cannot model the entire velocity field of practical flows. Because of this serious limitation of these similarity solutions, the practical applicability of the feature, that $C_p$ has a sharp minimum, needs further theoretical and experimental studies.

## IX. CONCLUSIONS

(1) A common feature of the $\mathbf{v}\sim z^{-n}$ jets is the twofold dependence on swirl number $Sw$: for any $n$, two solutions exist for $Sw<Sw_f$ and no solution exists for $Sw>Sw_f$.
(2) As $Sw$ decreases along the upper branch, the flow becomes more consolidated near the axis and the role of swirl diminishes.
(3) As $Sw$ decreases along the lower branch, the flow becomes two cellular. The role of swirl is crucial for this flow development despite the fact that $Sw$ is small.
(4) As $Sw$ further decreases, the flow inside the separation zone becomes swirl-free and irrotational.
(5) Neither the analytical continuation nor the stagnation zone model is valid for these flows.
(6) The thickness of the separation zone is bounded in the boundary layer scale for $n>1$, but can become of $O(1)$ for $n\leqslant 1$.
(7) The pressure coefficient has the sharp minimum at $Sw\approx 0.65$ in a wide range of $n$. The corresponding flow is the annular jet without flow reversal.

## ACKNOWLEDGMENTS

NSF Grant Nos. CTS-9622302 and CTS-9904328 supported this study which was partially performed at the University of Bristol, funded by the EPSRC Grant No. GR/L5 7692 (England) and by the DGICYT Grant No. PB93-0974-C02-02 (Spain). The authors cordially thank Professor Philip Drazin for his support and discussion.

[1]T. Sarpkaya, ''Vortex breakdown in swirling conical flows,'' AIAA J. **9**, 1792 (1971).
[2]M. P. Escudier, ''Observation of the flow produced in a cylindrical container by a rotating endwall,'' Exp. Fluids **2**, 189 (1984).
[3]O. R. Burggraf and M. R. Foster, ''Continuation or breakdown in tornado-like vortices,'' J. Fluid Mech. **80**, 685 (1977).
[4]M. A. Goldshtik, ''Viscous flow paradoxes,'' Annu. Rev. Fluid Mech. **22**, 441 (1990).
[5]M. V. Lowson, ''Some experiments with vortex breakdown,'' J. R. Aeronaut. Soc. **68**, 343 (1964).
[6]M. G. Hall, ''A theory for the core of a leading-edge vortex,'' J. Fluid Mech. **11**, 209 (1961).
[7]R. R. Long, ''A vortex in an infinite viscous fluid,'' J. Fluid Mech. **11**, 611 (1961).
[8]V. Shtern and F. Hussain, ''Hysteresis in swirling jets,'' J. Fluid Mech. **309**, 1 (1996).
[9]H. Schlichting, *Boundary-Layer Theory* (McGraw-Hill, New York, 1979); see also H. Schlichting and K. Gersten, *Grenzschicht-Theorie*, 9. Aufl. (Springer, Berlin, 1997).
[10]M. G. Hall, ''A new approach to vortex breakdown,'' Proceedings of the Heat Transfer and Fluid Mechanics Institute, University of California San Diego, La Jolla, 319, 1967.
[11]R. Fernandez-Feria, J. Fernandez de la Mora, and A. Barrero, ''Solution breakdown in a family of self-similar vortices,'' J. Fluid Mech. **307**, 77 (1995).
[12]M. Menke and I. Gursul, ''Unsteady nature of leading edge vortices,'' Phys. Fluids **9**, 2960 (1997).
[13]C. Brüker and W. Althaus, ''Study of vortex breakdown by particle tracking velocimetry (PTV),'' Exp. Fluids **13**, 339 (1992).
[14]M. P. Escudier, ''Vortex breakdown and the criterion for its occurrence,'' in *Topics in Atmospheric and Oceanographic Sciences*, edited by Bengtsson/Lighthill (Springer-Verlag, Berlin, 1982), pp. 247–258.
[15]J. J. Keller, W. Egli, and R. Athaus, ''Vortex breakdown as a fundamental element of vortex dynamics,'' ZAMP **39**, 404 (1988).
[16]R. Fernandez-Feria, J. Fernandez de la Mora, M. Perez-Saborid, and A. Barrero, ''Conically similar swirling flows at high Reynolds numbers,'' Quarterly J. Mech. Appl. Math. **52**, 1 (1999).
[17]T. B. Benjamin, ''Theory of the vortex breakdown phenomenon,'' J. Fluid Mech. **14**, 593 (1962).
[18]J. J. Keller, ''On the interpretation of vortex breakdown,'' Phys. Fluids **7**, 1695 (1995).
[19]S. Wang and Z. Russak, ''The dynamics of a swirling flow in a pipe and transition to axisymmetric vortex breakdown,'' J. Fluid Mech. **340**, 177 (1997).
[20]M. A. Goldshtik, *Vortex Flows* (Nauka, Novosibirsk, 1981), p. 277.
[21]I. I. Smulsky, *Aerodynamics and Processes in Vortex Chambers* (Nauka, Novosibirsk, 1992), p. 93.
[22]M. R. Foster and F. T. Smith, ''Stability of Long's vortex at large flow force,'' J. Fluid Mech. **206**, 405 (1989).
[23]T. Surpkaya, ''Turbulent vortex breakdown,'' Phys. Fluids **7**, 2301 (1995).
[24]E. Meissel, ''Über den Ausfluss der Wasser aus Gefässen in zwei besonderen Fällen nach Eintritt des Beharrungszustandes,'' Archiv der Mathematik und Physik, Bd. **55** (1873).
[25]S. Leibovich, ''Vortex stability and breakdown: Survey and extensions,'' AIAA J. **22**, 1192 (1984).
[26]M. Goldshtik and F. Hussain, ''The nature of inviscid vortex breakdown,'' Phys. Fluids **9**, 263 (1997).
[27]P. B. Earnshow, ''An experiment investigation the structure of a leading-edge vortex,'' Aeronaut. Res. Council Rep. **22**, 876 (1961).
[28]T. Surpkaya and F. Novak, ''Turbulent vortex breakdown: Experiments in tubes at high Reynolds numbers,'' in *Dynamics of Slender Vortices*, edited by E. Krause and K. Gersten (Kluwer, Dordrecht, 1998), pp. 287–296.
[29]V. Shtern, A. Borissov, and F. Hussain, ''Vortex sinks with axial flow: Solution and applications,'' Phys. Fluids **9**, 2941 (1997).
[30]A. Spohn, M. Mory, and E. J. Hopfinger, ''Experiments on vortex breakdown in a confined flow generated by a rotating disc,'' J. Fluid Mech. **370**, 73 (1998).
[31]P. Billant, J.-M. Chomaz, and P. Huerre, ''Experimental study of vortex breakdown in swirling jets,'' J. Fluid Mech. **376**, 183 (1998).